# Space geodesy validation of the global lithospheric flow

M. Crespi,[1] M. Cuffaro,[2] C. Doglioni,[2] F. Giannone[1] and F. Riguzzi[2,3]

[1]*DITS – Area di Geodesia e Geomatica, Università di Roma 'La Sapienza', Roma. E-mail: mattia.crespi@uniroma1.it*
[2]*Dipartimento di Scienze della Terra, Università di Roma 'La Sapienza', Roma. E-mail: carlo.doglioni@uniroma1.it*
[3]*Istituto Nazionale di Geofisica e Vulcanologia, sez. CNT, Roma. E-mail: riguzzi@ingv.it*

**SUMMARY**
Space geodesy data are used to verify whether plates move chaotically or rather follow a sort of tectonic mainstream. While independent lines of geological evidence support the existence of a global ordered flow of plate motions that is westerly polarized, the Terrestrial Reference Frame (TRF) presents limitations in describing absolute plate motions relative to the mantle. For these reasons we jointly estimated a new plate motions model and three different solutions of net lithospheric rotation. Considering the six major plate boundaries and variable source depths of the main Pacific hotspots, we adapted the TRF plate kinematics by global space geodesy to absolute plate motions models with respect to the mantle. All three reconstructions confirm (i) the tectonic mainstream and (ii) the net rotation of the lithosphere. We still do not know the precise trend of this tectonic flow and the velocity of the differential rotation. However, our results show that assuming faster Pacific motions, as the asthenospheric source of the hotspots would allow, the best lithospheric net rotation estimate is $13.4 \pm 0.7$ cm yr$^{-1}$. This superfast solution seems in contradiction with present knowledge on the lithosphere decoupling, but it matches remarkably better with the geological constraints than those retrieved with slower Pacific motion and net rotation estimates. Assuming faster Pacific motion, it is shown that all plates move orderly 'westward' along the tectonic mainstream at different velocities and the equator of the lithospheric net rotation lies inside the corresponding tectonic mainstream latitude band ($\approx \pm 7°$), defined by the $1\sigma$ confidence intervals.

**Key words:** lithospheric net rotation, plate kinematics, space geodesy, tectonic mainstream, Terrestrial Reference Frame, westward drift.

## 1 INTRODUCTION

A difficult task in geodynamics is the definition of a reference frame useful for the representation of plate motions, due to a number of kinematic uncertainties.

The most updated information on present plate motions is based on space geodesy data (Heflin *et al.* 2004), where the rate of motions are essentially estimated from GPS continuous observations (Fig. 1) in a NNR, as assumed by the International Terrestrial Reference Frame (ITRF2000) (Altamimi *et al.* 2002, 2003).

These data largely confirm the NNR-NUVEL1 data set, the Nuvel1 in a NNR frame, based on past ocean floor magnetic anomalies and focal mechanisms (DeMets *et al.* 1990; Argus & Gordon 1991), with a good match between past and present day plate motions (Stein 1993); therefore, it is assumed that present analysis is a good indicator of the main Cenozoic and Neozoic plate movements.

It is useful to recall that a Terrestrial Reference Frame (TRF) requires the definition of its scale, its origin and the orientation of the coordinate axes. The sensitivities of some techniques are better suited for observing certain aspects of the frame. For example, the scale of ITRF2000 is metric, depends on the speed of light because

the observing sites and the targets in the space are linked by electromagnetic signals and has been established by a combination of VLBI and SLR results. The TRF origin may be sensed by geodetic techniques; this has been realized in the geocentre, well defined by SLR observations. However, TRF orientation cannot be sensed by any geodetic technique, so that it is conventionally defined at a starting epoch and its time evolution is ensured by imposing the NNR condition over the whole Earth. The orientation of ITRF2000 has been aligned with the preceding realization, ITRF97, and its orientation rate is defined, by convention, so that there is NNR of the frame with respect to the Earth's lithosphere. To do so, the ITRF2000 orientation rate is aligned to the geological tectonic model NNR-NUVEL1A (Argus & Gordon 1991; DeMets *et al.* 1994). Clearly many of the geodetic sites are in plate boundary zones and thus were not used to specify the NNR condition. Sites whose velocities showed significant discrepancies with respect to NNR-NUVEL1A or with short observations were also removed from the rotational constraint. In practice, a subset of stations far from high deformation zones is selected to estimate the rotation parameters between ITRF and NNR-NUVEL1A velocities; finally, all site velocities have been rotated in the NNR-NUVEL1A system (Altamimi *et al.* 2002, 2003).
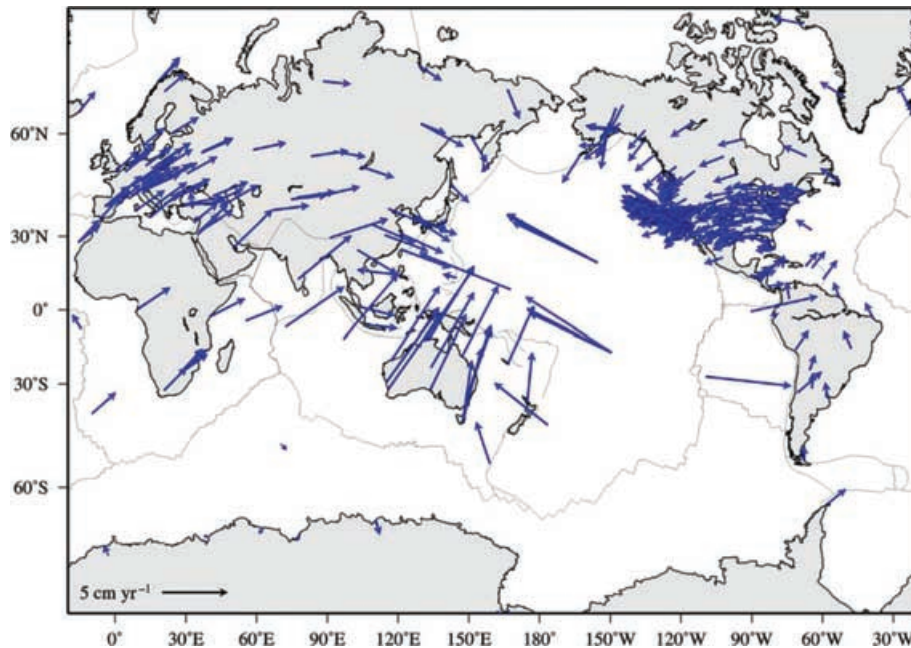
1

**Figure 1.** GPS NASA database of present-day plate motions (Heflin *et al.* 2004) in a NNR frame (ITRF2000).

Since the NNR hypothesis is an arbitrary choice introduced in order to fix the rank deficiency proper of the positions estimation problem based on space geodesy observations, this information is able to describe only for relative plate motions (Dermanis 2001, 2002), whereas any absolute motion relative to the mantle is not accounted for.

On the other hand, it is worth noting that the global analysis of tectonic features such as transform faults, subduction zones and rifts can also contribute to the present and past plate motions description. Using the major tectonic features on Earth, the plates appear not moving randomly, but they rather follow an undulated sinusoidal flow (Doglioni 1990, 1993), with possible (second-order) subrotations (Cuffaro *et al.* 2004). Moreover, plate motions are westerly polarized, the so-called net rotation or 'westward drift' (Le Pichon 1968; Bostrom 1971; O'Connell *et al.* 1991; Ricard *et al.* 1991) which can be evidenced both with respect to the Antarctica plate (Le Pichon 1968; Knopoff & Leeds 1972) as well as to the hotspot reference frame (HSRF) (Gordon 1995; Gripp & Gordon 2002). The existence of a westward drift polarizing the sinusoidal flow is also supported by independent geological and geophysical evidences, such as the asymmetry of subduction and rift zones following or opposing the relative counter motion of the mantle (Doglioni *et al.* 1999, 2003).

The main purpose of this paper is to propose a unified way to describe plate motions, overcoming the problems introduced by the NNR condition, taking into account that past and present plate kinematic analysis supports the existence of an ordered flow of plate motions which is polarized to the 'west' in the HSRF.

We propose an analytical description of the plate motions with respect to the underlying mantle, both accounting for relative plate kinematics inferred from space geodesy and first-order tectonic constraints. The concept of the tectonic mainstream is introduced (Section 2), and after a discussion on the westward drift of the lithosphere (Section 3), it is used to estimate plate motions and related global flow (Sections 4.1, 4.2 and 5).

## 2 THE TECTONIC MAINSTREAM

In order to establish the geological constraints for the definition of the analytical model, let us consider the six major plate boundaries of Earth (Pacific-Nazca, Nazca-South America, South-America-Africa, Africa-Arabia/India, Arabia/India-Eurasia, and Eurasia-Pacific) such as: the East Pacific Rise, the Mid-Atlantic ridge, and the Red Sea - Indian ridge, for extensional margins, and the western Pacific subduction zones, the western northern and southern Americas Cordilleras, and the Alpine–Himalayas system for convergent margins (Fig. 2). In the extensional tectonic settings, we assume that transform faults are parallel to the relative plate motions, whereas in convergent settings, the relative plate motions are constrained by the dominant trend of folds and thrusts, where no significant transpressive tectonics occurs. Another prominent large scale plate boundary is the SW-Indian ridge which is not included in this present first-order analysis because it has very slow spreading rates and it is possibly related to the subrotations of Africa and Antarctica.

Starting from the Pacific WNW–ESE plate motion relative to the mantle and constrained by the Hawaiian and Society tracks, and moving ESE, the relative E-ward motion of the Nazca plate (in the NNR reference frame) can be transferred to an 'absolute' kinematic analysis. Continuing to the E, the motion of the Nazca plate relative to South America (Kendrick *et al.* 2003), allows to refer the motion of the South America again to the Pacific and so on. The major plate boundaries can then be connected in a global circuit. In this way it appears that plate motions describe a flow, exemplified by an imaginary line (Fig. 2), passing throughout all the major tectonic features of Earth.

This flow line crosses the EPR, where the rifting is about E–W, the Andean subduction (AS), the Middle Atlantic Ridge (MAR), again both almost E–W. Then the Red Sea and East Africa rift (RSEAR) open along the NE–SW trend, similarly to the Indian Ocean. The direction gradually moves to a NNE–SSW trend in
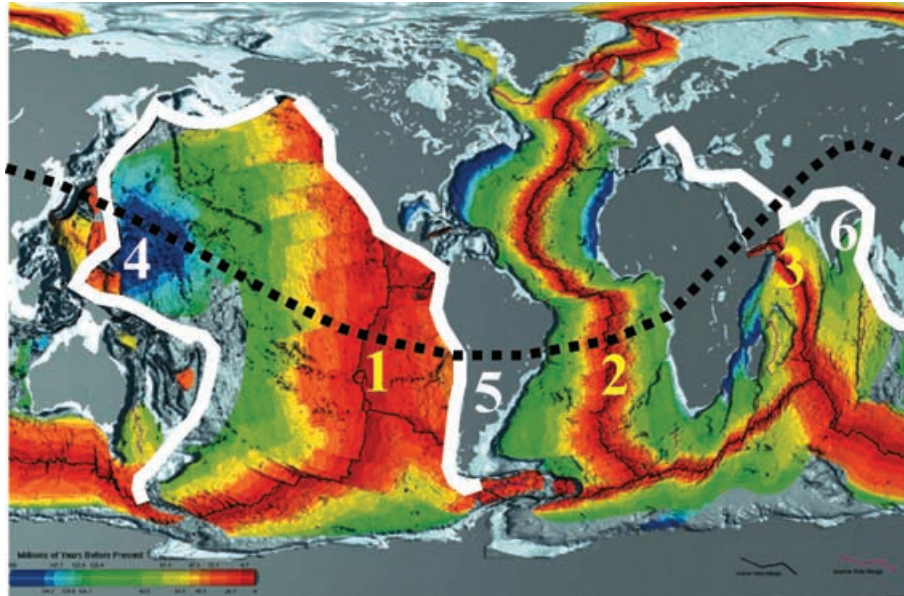
**Figure 2.** Construction of a tectonic mainstream, starting from the Pacific motion direction and linking all the other relative motions in a global circuit using first-order tectonic features such as the EPR (1), the Atlantic rift (2), the Red Sea, the Indian Ocean rift (3) for the rift zones, and the west Pacific subduction (4), the AS (5) and the Zagros-Himalayas Subduction and (6) for convergent margins . See text for description.

the Zagros-Himalayas (HimS) subduction zones. In Asia it rapidly turns to E–W and to NW–SE (Baikal rift, BR, and the Japan subduction, JS), eventually closing the circuit in the Pacific between the Hawaiian and Society Hotspots (HH) (Fig. 2). The flow line can be envisaged only filtering the transtensive or transpressive tectonic settings. For example, the East Africa Rift is characterized by left-lateral transtension where crossed by the flow line. Left-lateral transpression, as another example, characterizes the tectonic setting along the Chaman transform zone of Afghanistan–Pakistan where the NE–SW trending line enters into the Zagros-Himalayas orogens.

The flow line is stable back to at least 47 Myr (before the Hawaii-Emperor bending). However the Hawaii-Emperor bending has been shown not to be associated to a coeval rotation of the Pacific plate (Norton 1995). Moreover, apart minor oscillations, the flow seems to be stable since at least the Late Permian in the Atlantic rifting realm both in the earlier continental and later oceanic stages and along the Asian Cimmerides subduction zones. The trend inferred from these tectonic indicators is surprisingly coherent with the directions measured with space geodesy data in the NNR reference frame, apart in the MAR. However, when the net 'westward' rotation relative to the mantle is added, the match is more effective even in the MAR. Space geodesy data have been shown to be extremely comparable with past geological movements of the last million years (Stein 1993).

## 3 THE WESTWARD DRIFT OF THE LITHOSPHERE AND THE HSRF

In spite of its proven and accepted existence, the westward drift of the lithosphere has been not fully understood so that its implications are far to be applied: as relevant example, plate kinematics and space geodesy reference frames are still anchored to the no-net-rotation hypothesis (e.g. Argus & Gordon 1991; Heflin *et al.* 2004).

In particular, there still are doubts about (1) which is the engine of the westward drift, and (2) whether it affects the entire lithosphere or it is rather only a mean value, with most of the lithosphere moving

'west', but part of it still moving in the opposite direction relative to the mantle. According to this last opinion, only some plates would move westward, and since one of them is the Pacific plate, which is the largest and the fastest moving WNW-ward, the sum of all vectors would maintain a residual westward component, without a complete polarization (Ricard *et al.* 1991; Ranalli 2000). Regardless its nature and speed, combined with the hotspots tracks, the westward drift indicates the existence of a decoupling surface between lithosphere and subasthenospheric mantle.

The depth and nature of the hotspots source can help to unravel the question. In fact, the present debate on the shallow or deep mantle origin of the hotspots (Foulger *et al.* 2005) has a number of kinematic consequences in the HSRF. The hotspots may have different origin and variable depth source (e.g. Courtillot *et al.* 2003). For example some Atlantic hotspots have been interpreted as sourced from an asthenosphere richer in fluids, being in fact, cooler than other segments of the Mid-Atlantic Ridge, but wetter (Bonatti 1990). Some other Pacific intraplate hotspots have rather been interpreted as related to the shear heating generated at the decoupling interface between lithosphere and asthenosphere (Doglioni *et al.* 2005). Other shallow mechanisms that have been proposed are fissures or grabens in the lithosphere (Natland & Winterer 2005; Anderson 2005) but other segments of the scientific community still prefers to interpret hotspots as deep mantle features (e.g. Morgan 1971; Davies 1988) or intermediate sources (e.g. Ritsema & Allen 2003). Therefore, magmatic trails or hotspots tracks at the surface could have different origins and depth source, although they are still often erroneously mixed together or considered as a single system. However, to the aim of this research, the depth of the hotspots and the screening of their kinematic reliability are critical in order to have a realistic reference frame of lithospheric motion relative to the mantle.

There are a number of growing evidences suggesting that the so-called hotspots are rather superficial features, sourced either from the asthenosphere, or the lithosphere base itself (Bonatti 1990; Smith 1993; Smith & Lewis 1999; Anderson 2000), possibly unrelated to deep mantle sources.

Since most of the hotspots, are steadily located on ridges, rift zones or transform zones, and plate kinematics requires ridges moving relative to the underlying mantle, this means they should be sourced either from the asthenosphere or above it. For example, oceanic ridges are moving one respect to the other, like the Atlantic and Indian ridges, which are moving away from Africa; therefore, 'hotspots' which are persistently located along or close to oceanic ridges (e.g. Azores, Ascension, Tristan da Cuna, Galapagos) cannot be considered fixed. In other words, they are detached from the mantle and they do not represent either a reliable fixed frame for measuring plate motions, or an indication of the movements in the underlying mantle. Therefore, the present HSRF might not be a suitable reference frame for the absolute plate motions representation.

However, the main Pacific hotspots are located within the plate and they appear as unrelated to plate margins dynamics. Moreover, these hotspots are fixed relative to each other (Gripp & Gordon 2002), and their motion coincides with the direction of the Pacific plate detected at the East Pacific Rise. For these reasons, the Pacific hotspots can be taken as a reference frame for global plate motions computation, what will be considered in Section 6.

As an example, Gripp & Gordon (2002) defined the last hotspot reference frame HS3-NUVEL1A, using eleven segment trends and two volcanic propagation rates as constraints and estimating a set of angular velocities consistent with the relative plate motions model NUVEL1A (DeMets *et al.* 1990, 1994).

Since the source depth of hotspots or plumes is under debate (Foulger *et al.* 2005), whether hotspots are sourced either from the deep mantle or the asthenosphere, the relative motion between lithosphere and mantle assumes opposite end-member velocities. The slowest decoupling occurs for deep hotspots, whereas the fastest decoupling is for shallow plumes. Therefore, two hotspots reference frames can be described, depending on the source depth of the magmatism. For example, the shallow source model of hotspots located in the middle of the asthenosphere almost doubles the decoupling between lithosphere and subasthenospheric mantle in the Pacific (from 10 to 20 cm yr$^{-1}$), raising the westward drift to a complete polarization (Doglioni *et al.* 2005).

## 4 PLATE MOTION KINEMATIC MODEL

The wide use of space geodesy techniques devoted to geophysical and geodynamic purposes has recently evidenced some limitations due to the intrinsic TRF definition. It is noteworthy that current reference frames based on space geodesy techniques (ITRF2000) are defined under hypotheses suited to overcome the rank deficiency of the observations with respect to the parameters that have to be estimated, that is, coordinates and velocities (Dermanis 2001, 2002). From a geodetic point of view, one possibility implies the application of the no-net-rotation condition (NNR) (Altamimi *et al.* 2003). This condition is realized by aligning the global intertechnique ITRF2000 solutions to the NNR-NUVEL1A model (i.e. by imposing null rotation rate components between ITRF2000 and NNR-NUVEL1A). The application of this condition, besides the known limitations (Dermanis 2002; Altamimi *et al.* 2003), has heavy geophysical consequences; in fact, ITRF2000 allows for accurate estimations of relative plate motions only (Altamimi *et al.* 2003), whilst any absolute motion (for instance, with respect to the inner layers of the Earth body, in particular the mantle) is not determinable.

In this study, we try to overcome such limitations introduced by the application of the NNRC, starting from a simple global kinematic model in which we introduce the net rotation of the lithosphere with respect to the mantle.

Particularly, we hypothesize that each plate motion may be mainly described by a first-order term, accounting for the net ordered rotation at global scale (represented by an angular velocity vector different from plate to plate), and a second-order term, accounting for possible plate subrotations (Cuffaro *et al.* 2004), which is here neglected. First-order plate motion follows an imaginary line representing their main trajectory (tectonic mainstream), according to what discussed in Section 2; this line may allow a simple analytical representation as a low (e.g. third-) order Fourier series in geographic coordinates $(\varphi, \lambda)$

$$\varphi(\lambda) = \frac{a_0}{2} + \sum_{i=1}^{3} [a_i \cos(i\lambda) + b_i \sin(i\lambda)]. \tag{1}$$

The seven parameters in eq. (1) may be computed starting from the concept of Eulerian equator plane of each plate, which is just the plane orthogonal to plate absolute (w.r.t. the mantle) angular velocity; in a spherical Earth approximation, all absolute angular plate velocities pass through the Earth centre as their correspondent Eulerian equatorial planes (Fig. 3). If we consider all the plates crossed by the *mainstream* and the traces of their Eulerian equatorial planes on the sphere (Eulerian equators), the tectonic mainstream line may be regarded as the line globally approximating the Eulerian equators themselves. Therefore, the seven parameters in eq. (1) may be derived after absolute angular velocities estimation, as described in Section 6.

In order to set up the model to perform this estimation, we start from the transformation between two velocity sets (NNR and HSRF), which reads

$$\vec{V} = \vec{V}_{\mathrm{NNR}} + \vec{V}_d, \tag{2}$$

where $\vec{V}$ is the absolute (i.e. HSRF), $\vec{V}_{\mathrm{NNR}}$ is the NNR velocity whose components are $(V_{X_{\mathrm{NNR}}}, V_{Y_{\mathrm{NNR}}}, V_{Z_{\mathrm{NNR}}})$ and $\vec{V}_d$ is the drag term, due to the net-rotation of lithosphere with respect to the mantle.

Let us consider for simplicity $P$ plates with $i$ sites, thus we can expand eq. (2) in terms of the absolute angular velocity $\vec{\omega}^p$ and
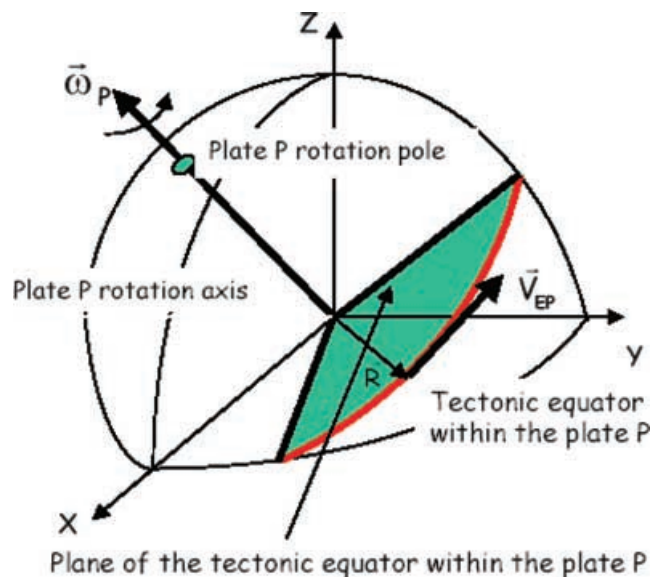


**Figure 3.** Kinematic condition between tectonic mainstream (red line) and angular velocity of a given plate, under spherical approximation.

geocentric position $\vec{r}_i$ as

$$\vec{\omega}^p \times \vec{r}_i - \vec{\omega}^d \times \vec{r}_i = \vec{V}_{i_{NNR}}, \tag{3}$$

where $\vec{\omega}^d$ is the drag angular velocity.

We recall that

$$\vec{V} = \vec{\omega} \times \vec{r} \text{ has components } \begin{vmatrix} V_X \\ V_Y \\ V_Z \end{vmatrix} = \det \begin{vmatrix} i & j & k \\ \omega_X & \omega_Y & \omega_Z \\ X & Y & Z \end{vmatrix}$$

with $i$, $j$, $k$ versors of $X$, $Y$, $Z$ axes, so that

$$V_X = Z \cdot \omega_Y - Y \cdot \omega_Z$$

$$V_Y = X \cdot \omega_Z - Z \cdot \omega_X$$

$$V_Z = Y \cdot \omega_X - X \cdot \omega_Y$$

or, equivalently, separating the $\vec{\omega}$ components,

$$\begin{vmatrix} V_X \\ V_Y \\ V_Z \end{vmatrix} = \begin{vmatrix} 0 & Z & -Y \\ -Z & 0 & X \\ Y & -X & 0 \end{vmatrix} \cdot \begin{vmatrix} \omega_X \\ \omega_Y \\ \omega_Z \end{vmatrix}$$

Hence, the relationship (3) in matricial form becomes

$$\begin{vmatrix} 0 & Z_i^p & -Y_i^p \\ -Z_i^p & 0 & X_i^p \\ Y_i^p & -X_i^p & 0 \end{vmatrix} \cdot \left( \begin{vmatrix} \omega_X^p \\ \omega_Y^p \\ \omega_Z^p \end{vmatrix} - \begin{vmatrix} \omega_X^d \\ \omega_Y^d \\ \omega_Z^d \end{vmatrix} \right) = \begin{vmatrix} V_{X_i} \\ V_{Y_i} \\ V_{Z_i} \end{vmatrix}_{NNR} \tag{4}$$

This model explicitly relates plate absolute angular velocities $\vec{\omega}^p$, drag angular velocity $\vec{\omega}^d$ (net-rotation angular velocity) and velocity 'observed' by GPS under NNR condition at some selected ITRF2000 sites.

It clearly shows a rank deficiency with respect to the angular velocities in sense that one of them has to be fixed in order to estimate the others, being equal the velocity differences; in particular, it is easy to verify that, if the arbitrary vector

$$n = \begin{vmatrix} \Delta\omega_X \\ \Delta\omega_Y \\ \Delta\omega_Z \end{vmatrix}$$

is added to all (plate and drag) absolute angular velocities, the left-hand side of eq. (4) does not change.

On the other hand, we can fix the rank deficiency by introducing suitable additional constraints on the absolute plate angular velocities ($\vec{\omega}^a$, $\vec{\omega}^b$), what may be done under the hypothesis of the existence of a tectonic mainstream representing the first-order absolute plate motions.

These constraints regard:

(1) Continuity of the Eulerian equators, that is, they must connect each others at plate boundaries.

(2) Azimuths of the Eulerian equators at some longitudes, mainly forced by the principal tectonic features.

(3) Attitude (and its precision) of the Pacific plate Eulerian equatorial plane, based on the motion directions (azimuths) of two well-recognized hotspots within the Pacific plate (Hawaii and Society Islands).

(4) Velocities of Hawaii and Society Islands hotspots, based on different hypotheses of their source depths (deep mantle or mid-asthenosphere).

## 4.1 Continuity of the Eulerian equators

Since the Eulerian equator plane of each plate is orthogonal to plate absolute angular velocity and they cross in the Earth centre, Eulerian equator plane equation in the geocentric Cartesian coordinates system reads

$$\omega_X X + \omega_Y Y + \omega_Z Z = 0, \tag{5}$$

where, in spherical approximation (mean Earth radius $R = 6371$ km)

$$\begin{vmatrix} X \\ Y \\ Z \end{vmatrix} = R \begin{vmatrix} \cos\varphi \cos\lambda \\ \cos\varphi \sin\lambda \\ \sin\varphi \end{vmatrix},$$

therefore, eq. (5) in geographic coordinates ($\varphi, \lambda$) becomes

$$\omega_X \cos\varphi \cos\lambda + \omega_Y \cos\varphi \sin\lambda + \omega_Z \sin\varphi = 0. \tag{6}$$

This equation is just useful to write down continuity constraints; in fact, at the boundary between plates a and b ($\varphi^{ab}, \lambda^{ab}$) (note that in our model intersection between each plate boundary and plate Eulerian equator is represented by a point) continuity condition states that

$$\omega_X^a \cos\varphi^{ab} \cos\lambda^{ab} + \omega_Y^a \cos\varphi^{ab} \sin\lambda^{ab} + \omega_Z^a \sin\varphi^{ab}$$
$$= \omega_X^b \cos\varphi^{ab} \cos\lambda^{ab} + \omega_Y^b \cos\varphi^{ab} \sin\lambda^{ab} + \omega_Z^b \sin\varphi^{ab} \tag{7a}$$

or, under the hypothesis (in our case always satisfied) that $\cos\varphi^{ab} \neq 0$ ($\varphi^{ab} \neq \pm\frac{\pi}{2}$) and $\omega_Z^a, \omega_Z^b \neq 0$

$$\cos\lambda^{ab} \frac{\omega_X^a}{\omega_Z^a} + \sin\lambda^{ab} \frac{\omega_X^a}{\omega_Z^a} = -\tan\varphi^{ab}$$
$$\cos\lambda^{ab} \frac{\omega_X^b}{\omega_Z^b} + \sin\lambda^{ab} \frac{\omega_X^b}{\omega_Z^b} = -\tan\varphi^{ab} \tag{7b}$$

more useful form the computational point of view; in this respect it has to be underlined that eq. (7a) or the equivalent system (7b) are not linear with respect to the unknown parameters to be estimated ($\omega_X^a$, $\omega_Y^a$, $\omega_Z^a$, $\omega_X^b$, $\omega_Y^b$, $\omega_Z^b$, $\varphi^{ab}$, $\lambda^{ab}$); the necessary approximated values are supplied joining information stemming from geology and space geodesy.

## 4.2 Azimuth constraints on the Eulerian equators

The second kind of constraints interprets an additional geological condition that, in our opinion, must be satisfied: the tectonic mainstream direction must be equal to the mean azimuth $\alpha$ of motion across the largest Earth crust tectonic discontinuities (Gordon 1995; Searle 1986) (Table 1, Fig. 4), as reported in detail in Section 2.

Therefore, again representing with one point the intersection between the Eulerian equator and a tectonic discontinuity, the second

**Table 1.** Azimuth of the selected tectonic features.

|   | $\lambda$ (°) | $\varphi$ (°) | $\alpha$ (°) |
|---|---|---|---|
| 1 | 348 | −29 | 74 ± 3 |
| 2 | 56 | 12 | 40 ± 3 |
| 3 | 80 | 33 | 61 ± 3 |
| 4 | 142 | 35 | 103 ± 5 |
| 5 | 195 | 16 | 109 ± 5 |
| 6 | 245 | −17 | 113 ± 3 |
| 7 | 288 | −25 | 99 ± 5 |

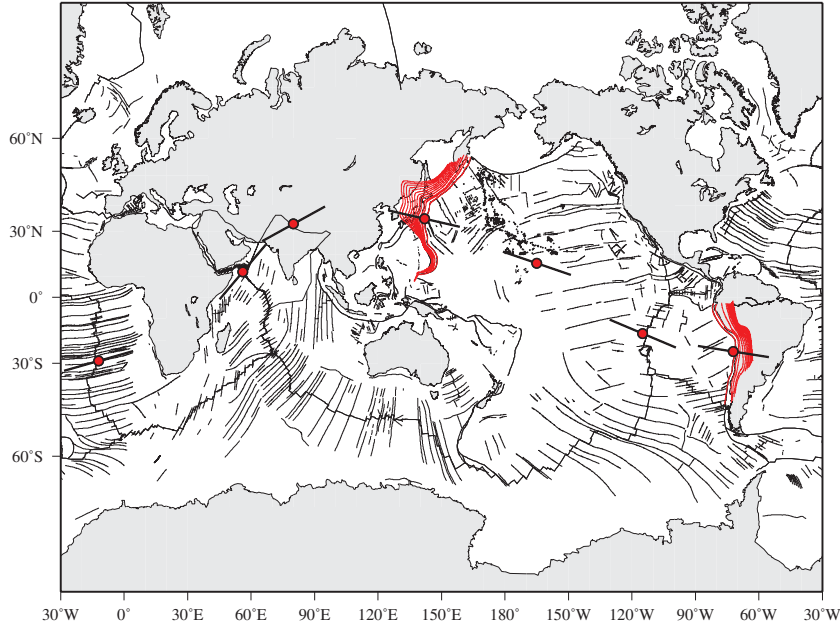*Note*: 1: MAR; 2: RSEAR; 3: HimS; 4: JS; 5: HH ; 6: EPR and 7: AS.

**Figure 4.** Map of the main tectonic features (listed in Table 1) selected to introduce azimuth constraints into the tectonic mainstream estimation.

kind of constraints states that Eulerian equator azimuth has known value $\alpha^t$ in some selected points $(\varphi^t, \lambda^t)$ (Table 1, Fig. 4). By applying simple geometric considerations, azimuth constraint equation reads

$$\sin \lambda^t \cos \varphi^t \frac{\omega_X}{\omega_Z} - \cos \lambda^t \cos \varphi^t \frac{\omega_Y}{\omega_Z} = \cot \alpha^t. \tag{8}$$

Note that if the discontinuity coincides with a plate boundary, eq. (8) must be satisfied on both sides, that is for both plates a and b

$$\sin \lambda^t \cos \varphi^t \frac{\omega_X^a}{\omega_Z^a} - \cos \lambda^t \cos \varphi^t \frac{\omega_Y^a}{\omega_Z^a} = \cot \alpha^t$$

$$\sin \lambda^t \cos \varphi^t \frac{\omega_X^b}{\omega_Z^b} - \cos \lambda^t \cos \varphi^t \frac{\omega_Y^b}{\omega_X^b} = \cot \alpha^t$$

in this case, the two equations constraint both azimuth and continuity at the plate boundary.

### 4.3 Attitude of the Pacific plate Eulerian equatorial plane

The attitude of the Pacific plate Eulerian equatorial plane in terms of absolute angular velocity components ratios $(\frac{\omega_X}{\omega_Z}, \frac{\omega_Y}{\omega_X})$ may be derived with its approximated uncertainty (angular velocity components ratio standard deviations) by eq. (8), on the basis of the data concerning the motion azimuths of two well-recognized hotspots within the Pacific plate (Hawaii and Society Islands) published in the interesting paper of Gripp & Gordon (2002, Table 11). As regards attitude precision, note that azimuths of the observed trend for these hotspots show the best precision in the whole hotspots
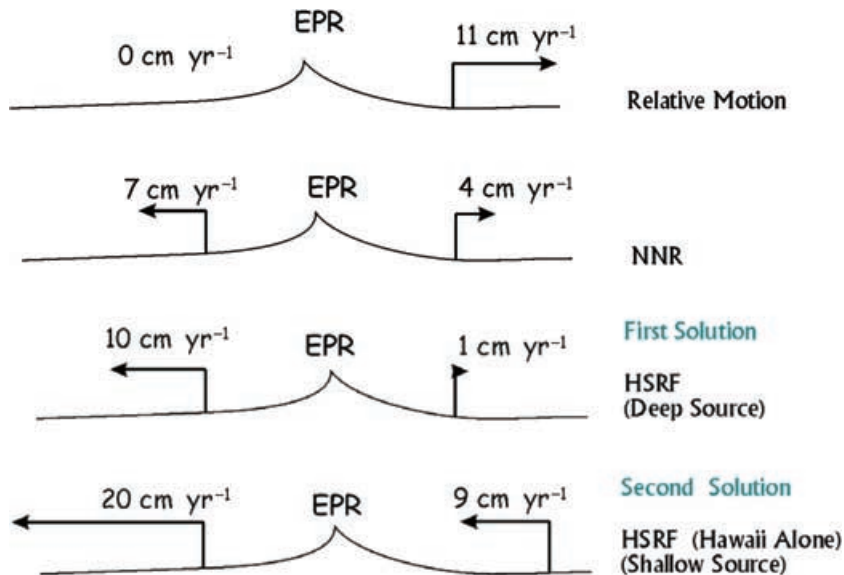


**Figure 5.** Example of East Pacific Rise plate kinematics; from top to bottom: relative motion, NNR motion, HSRF first solution, HSFR (Hawaii) second solution (after Doglioni *et al.* 2005).

set, consequently we prefer to base our present modelling on this conservative choice. Then, recalling eq. (8) and applying covariance propagation law under the hypothesis that angular velocity components ratio are independent, we may write down two equations for Hawaii (superscript H) and Society Islands (superscript S), respectively,

$$(\sin \lambda^H \cos \varphi^H)^2 \sigma^2 \left( \frac{\omega_X}{\omega_Z} \right)_{PA} - (\cos \lambda^H \cos \varphi^H)^2 \sigma^2 \left( \frac{\omega_Y}{\omega_Z} \right)_{PA}$$
$$= \frac{1}{\sin^4 \alpha^H} \sigma^2 (\alpha^H)$$
$$(\sin \lambda^S \cos \varphi^S)^2 \sigma^2 \left( \frac{\omega_X}{\omega_Z} \right)_{PA} - (\cos \lambda^S \cos \varphi^S)^2 \sigma^2 \left( \frac{\omega_Y}{\omega_Z} \right)_{PA}$$
$$= \frac{1}{\sin^4 \alpha^S} \sigma^2 (\alpha^S) \tag{9}$$

in the two unknowns $\sigma(\frac{\omega_X}{\omega_Z})_{PA}$ and $\sigma(\frac{\omega_Y}{\omega_Z})_{PA}$.

## 4.4 Velocities of Hawaii and Society Islands hotspots

Different velocities for Hawaii and Society Islands hotspots with respect to the mantle may be hypothesized on the basis of different source depths. As example, we show in Fig. 5 a simple sketch of the East Pacific Rise (EPR) plate kinematics, where it is easy to observe that the same relative motion may lead to different absolute velocities according to the different hypothesis, NNR, deep and shallow hotspot source depths (Doglioni *et al.* 2005). This constraint may be simply given by $\omega_Z$ component of Pacific plate absolute angular velocity since components ratios $(\frac{\omega_X}{\omega_Z}, \frac{\omega_Y}{\omega_X})$ with their precisions are already constrained by eq. (8), as above discussed.

## 5 KINEMATIC PARAMETERS ESTIMATION

Having exploited both the pure rank deficient kinematic model (4) and the constraints (7) and (8) which play a relevant role in the plate and drag absolute angular velocities determination, all the parameters involved in the model (plate and drag absolute angular velocities themselves, together with geographic coordinates of points at plate boundaries where Eulerian equators continuity condition is imposed) may be estimated according to the least-squares principle, starting from approximated values being the model non-linear.

In this respect, the solution was carried out iteratively in a two-steps procedure.

First of all, eqs (8) were written for the six boundaries between plates crossed by tectonic mainstream, plus the mean azimuth of the Hawaii and Society Islands motions; these equations were solved separately from eqs (4), in order to estimate the unknowns plate absolute angular velocity components ratios which fulfill both azimuths and continuity constraints ($\tilde{\omega}_{XZ} = (\frac{\omega_X}{\omega_Z})_{ac}$, $\tilde{\omega}_{YZ} = (\frac{\omega_Y}{\omega_Z})_{ac}$), starting from approximated values of geographic coordinates of points at plate boundaries where Eulerian equators continuity condition is imposed.

Then pseudo-observation equations on absolute angular velocity components of the form:

$$\omega_X = \tilde{\omega}_{XZ} \omega_Z$$
$$\omega_Y = \tilde{\omega}_{YZ} \omega_Z \tag{10}$$

are added to eqs (4) to solve the global model, estimating plate and drag absolute angular velocities.

The general (linear) form of the model for the second step reads

$$Y_0 + v = Ax \text{ (functional model)}$$

$$C_{y_0 y_0} = \sigma_0^2 Q \text{ (stochastic model)},$$

where $Y_o$ is the pseudo-observation vector, $v$ is the residuals vector, A is the design matrix, $x$ is the parameters vector, $C_{y_0 y_0}$ is the observations covariance matrix, $\sigma_0^2$ is the prior variance of unit weight and $Q$ is the observations cofactor matrix.

As regards the functional model, eqs (4) were written for 28 GPS sites located on major plates (three for Pacific, Eurasia, India, Africa, South America, North America, Australia and Antarctica, two for Nazca and Arabia, the only available on these plates) far from high deformation areas, so that all plates involved has a similar number of sites. The selected sites have long enough coordinate time-series, useful to manage reliable ITRF2000 velocity components. Table 2 shows the list of sites and the corresponding ITRF2000 velocities according to the solution provided by JPL (Heflin *et al.* 2004).

Moreover, the pseudo-observation eqs (10) were written for the six plates crossed by tectonic mainstream. Finally, one more pseudo-observation equation on $\omega_Z$ component of Pacific plate absolute angular velocity is added, constraining this parameter to a value driven by the hypothesis about hotspot source depths (Doglioni *et al.* 2005).

As regards the stochastic model, in order to assess both the mean inner precision of the pure kinematic model and the reliability of the selected GPS sites, a preliminary adjustment with $\vec{\omega}^d = 0$ and $Q = I$ was performed; in this respect it has to be recalled that velocity precisions estimated in ITRF2000 realization are overestimated by far (usually of the order of tenths of mm yr$^{-1}$), as discussed in Barzaghi *et al.* (2004). The variance of unit weight was re-estimated, resulting $\hat{\sigma}_0 = 2.8$ mm yr$^{-1}$, coherently with results in Barzaghi *et al.* (2004); this value was used as prior one into the global estimation procedure. Moreover, eqs (9) supplied the two unknowns:

$$\sigma \left( \frac{\omega_X}{\omega_Z} \right)_{PA} \cong 0.15$$
$$\sigma \left( \frac{\omega_Y}{\omega_Z} \right)_{PA} \cong 0.17. \tag{11}$$

Then, the full stochastic model was defined, considering all equations independent. For pure kinematic eqs (4), the variance was just set equal to $\hat{\sigma}_0^2$. For the pseudo-observation equations (10) variance was derived by the well-known variance propagation law, from (11) and accounting both $\sigma(\omega_Z)_p$ uncertainties (iteratively estimated for each plate p) and the areas ratio $\frac{A_p}{A_{PA}}$ between each plate p and the Pacific one (Schettino 1999):

$$\sigma \left( \frac{\omega_X}{\omega_Z} \right)_p = \frac{A_p}{A_{PA}} \sigma \left( \frac{\omega_X}{\omega_Z} \right)_{PA}$$
$$\sigma \left( \frac{\omega_Y}{\omega_Z} \right)_p = \frac{A_p}{A_{PA}} \sigma \left( \frac{\omega_Y}{\omega_Z} \right)_{PA} \tag{12}$$

in this way we want to take into account that larger plate motions (Forsyth & Uyeda 1975) are likely to follow the first-order net rotation at global scale than narrower (which may experience significant subrotations here not considered), so that absolute angular velocity components ratios $(\frac{\omega_X}{\omega_Z}, \frac{\omega_Y}{\omega_X})$ derived at first step are as much reliable as wide plate is. Finally, $\dot{\omega}_Z$ for the Pacific plate was just fixed by a suitable high weight.

Table 2. Selected GPS sites, coordinates, velocities ITRF2000 and rms.

| PLATE | SITE | Latitude (°) | Longitude (°) | X (10⁶ m) | Y (10⁶ m) | Z (10⁶ m) | Vx (mm yr⁻¹) | sVx (mm yr⁻¹) | Vy (mm yr⁻¹) | sVy (mm yr⁻¹) | Vz (mm yr⁻¹) | sVz (mm yr⁻¹) |
|---|---|---|---|---|---|---|---|---|---|---|---|---|
| PA | MKEA | 19.801 | −155.456 | −5.4641052 | −2.4951665 | 2.1482912 | −14.850 | 0.10 | 63.040 | 0.06 | 31.070 | 0.04 |
| PA | KWJ1 | 8.722 | 167.730 | −6.1608809 | 1.3398834 | 0.9608107 | 21.760 | 0.32 | 66.810 | 0.16 | 27.410 | 0.08 |
| PA | THTI | −17.577 | −149.606 | −5.2464155 | −3.0772601 | −1.9138423 | −42.100 | 0.18 | 52.720 | 0.13 | 31.980 | 0.08 |
| NZ | EISL | −27.148 | −109.383 | −1.8849513 | −5.3575960 | −2.8928906 | 64.210 | 0.05 | −19.510 | 0.09 | −6.220 | 0.05 |
| NZ | GALA | −0.743 | −90.304 | −0.0337958 | −6.3775226 | −0.0821208 | 50.730 | 0.10 | 1.360 | 0.20 | 11.150 | 0.03 |
| SA | BOGT | 4.640 | −74.081 | 1.7443990 | −6.1160376 | 0.5127317 | −9.200 | 0.09 | 3.319 | 0.16 | 10.080 | 0.03 |
| SA | FORT | −3.877 | −38.426 | 4.9853866 | −3.9549986 | −0.4284264 | −2.920 | 0.08 | −4.530 | 0.07 | 11.940 | 0.02 |
| SA | RIOG | −53.785 | −67.751 | 1.4299078 | −3.4953548 | −5.1226987 | 6.800 | 0.08 | −10.620 | 0.11 | 2.710 | 0.15 |
| AF | MAS1 | 27.764 | −15.633 | 5.4391922 | −1.5220555 | 2.9534548 | −2.480 | 0.07 | 16.940 | 0.04 | 15.720 | 0.04 |
| AF | NKLG | 0.354 | 9.672 | 6.2873858 | 1.0715745 | 0.0391329 | −1.560 | 0.29 | 20.630 | 0.19 | 17.680 | 0.06 |
| AF | SUTM | −32.381 | 20.811 | 5.0411902 | 1.9160671 | −3.3971894 | 5.620 | 0.54 | 17.380 | 0.33 | 13.280 | 0.35 |
| AR | AMMN | 32.029 | 35.880 | 4.3861244 | 3.1726382 | 3.3636853 | −23.590 | 0.69 | 11.300 | 0.57 | 11.710 | 0.50 |
| AR | BAHR | 26.209 | 50.608 | 3.6339089 | 4.4252755 | 2.7998615 | −30.840 | 0.07 | 10.060 | 0.08 | 25.950 | 0.05 |
| EU | KUNM | 25.030 | 102.797 | −1.2812557 | 5.6407460 | 2.6828800 | −31.840 | 0.14 | 5.000 | 0.26 | −15.970 | 0.13 |
| EU | IRKT | 52.219 | 104.316 | −0.9683324 | 3.7944254 | 5.0181677 | −25.720 | 0.04 | 1.050 | 0.06 | −3.960 | 0.08 |
| EU | WTZR | 49.144 | 12.879 | 4.0755806 | 0.9318538 | 4.8015681 | −15.320 | 0.06 | 17.320 | 0.04 | 9.780 | 0.07 |
| IN | BAN2 | 13.034 | 77.512 | 1.3440877 | 6.0686103 | 1.4292919 | −34.960 | 0.61 | 1.267 | 1.10 | 35.470 | 0.34 |
| IN | HYDE | 17.417 | 78.551 | 1.2084446 | 5.9668060 | 1.8970768 | −35.240 | 0.93 | 1.120 | 1.88 | 32.620 | 0.72 |
| IN | IISC | 13.021 | 77.570 | 1.3379365 | 6.0703171 | 1.4278767 | −40.820 | 0.07 | 2.480 | 0.13 | 33.120 | 0.04 |
| AU | DARW | −12.844 | 131.133 | −4.0913591 | 4.6846067 | −1.4085801 | −35.380 | 0.17 | −13.010 | 0.18 | 53.820 | 0.07 |
| AU | PERT | −31.802 | 115.885 | −2.3686873 | 4.8813166 | −3.3417958 | −47.030 | 0.04 | 7.160 | 0.06 | 50.370 | 0.04 |
| AU | TOW2 | −19.269 | 147.056 | −5.0545829 | 3.2755044 | −2.0915394 | −31.680 | 0.16 | −13.250 | 0.12 | 50.330 | 0.07 |
| NA | ALGO | 45.956 | −78.071 | 0.9181294 | −4.3460713 | 4.5619778 | −16.340 | 0.03 | −4.610 | 0.04 | 3.390 | 0.04 |
| NA | MDO1 | 30.681 | −104.015 | −1.3299988 | −5.3283934 | 3.2365042 | −12.880 | 0.03 | −1.650 | 0.05 | −5.390 | 0.03 |
| NA | PRDS | 50.871 | −114.293 | −1.6596030 | −3.6767258 | 4.9254936 | −16.970 | 0.09 | −1.170 | 0.13 | −7.610 | 0.15 |
| AN | DAV1 | −68.577 | 77.973 | 4.8685455 | 2.2850993 | −5.9149557 | 0.820 | 0.04 | −5.280 | 0.05 | −3.480 | 0.10 |
| AN | VESL | −71.674 | −2.842 | 2.0093298 | −0.9974148 | −6.0331584 | 8.150 | 0.07 | −3.040 | 0.06 | 3.170 | 0.19 |
| AN | KERG | −49.351 | 70.256 | 1.4063373 | 3.9181611 | −4.8161674 | −5.460 | 0.07 | −0.380 | 0.10 | −4.060 | 0.11 |

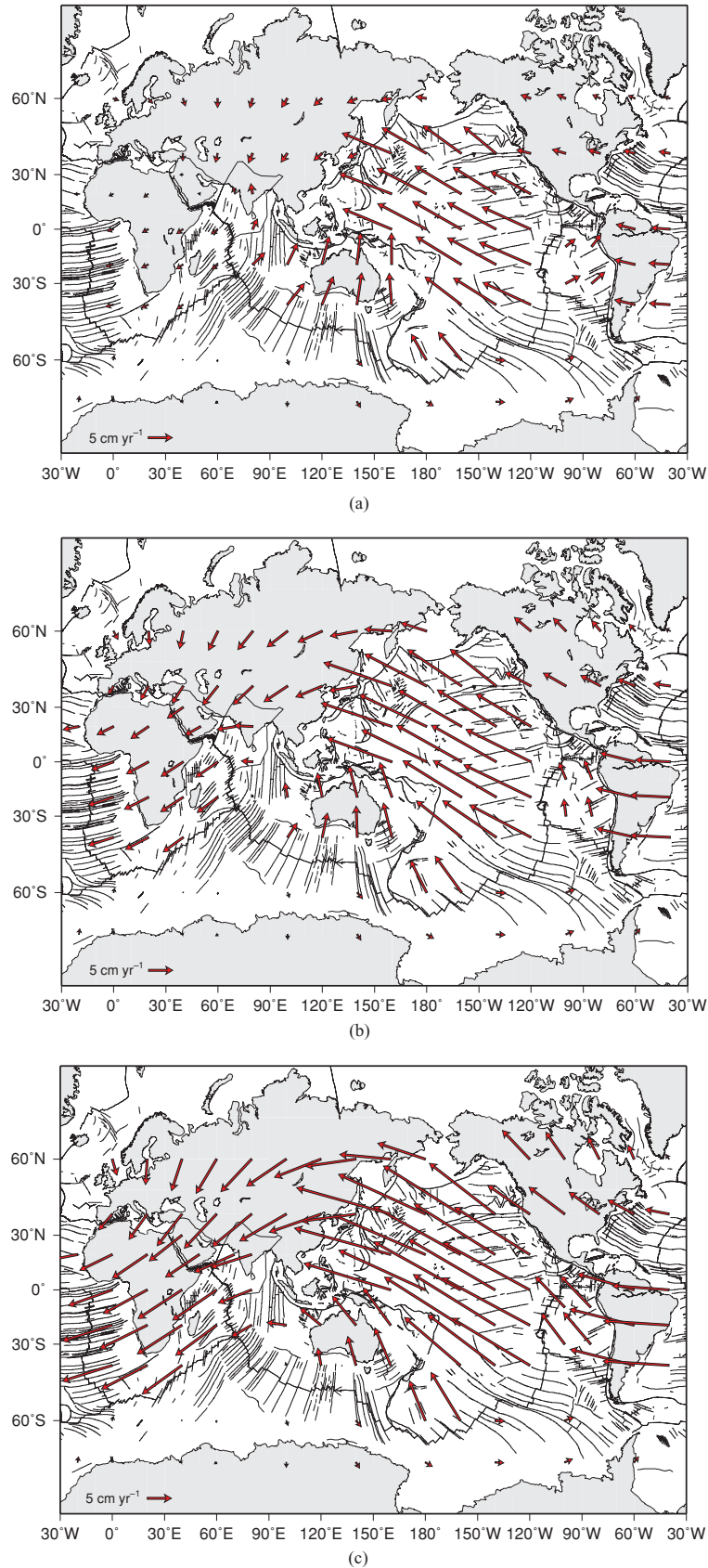**Figure 6.** Plate motions with respect to mantle flow (Table 3, 4): (a) GGS, lithosphere net rotation of 4.1 cm yr$^{-1}$ and maximum PA tangential velocity of 11.6 cm yr$^{-1}$; (b) S15, lithosphere net rotation of 8.0 cm yr$^{-1}$ and maximum PA tangential velocity of 15.5 cm yr$^{-1}$ and (c) S20, lithosphere net rotation of 13.4 cm yr$^{-1}$ maximum PA tangential velocity of 20.8 cm yr$^{-1}$.

## 6  PLATE KINEMATIC SOLUTIONS AND ANALYTICAL REPRESENTATION OF THE TECTONIC MAINSTREAM

As mentioned above, different hypotheses about the Pacific plate $\omega_Z$ component were considered, leading to the following three absolute plate kinematic solutions (Figs 6, 7 and 8; Tables 3 and 4).

(1) *Gripp and Gordon 'style' solution (GGS)*: The absolute angular velocity component $\omega_Z$ of the Pacific plate is chosen so that the prior maximum velocity within the Pacific plate (velocity along the Eulerian equator) is the same as in Gripp & Gordon (2002), about 11.2 cm yr$^{-1}$. Note that the posterior maximum velocity (Table 3) is slightly different since the uncertainties of the absolute angular velocity component ratios of the Pacific plate $(\frac{\omega_X}{\omega_Z})_{PA}$, $(\frac{\omega_Y}{\omega_X})_{PA}$ are accounted for, therefore, their values are estimated together all other

absolute angular velocity component ratios. This solution fulfils the global test on the model, in a Gaussian error fashion, with respect to the prior value $\hat{\sigma}_0 = 2.3$ mm yr$^{-1}$ at the 95 per cent significance level

$$r\frac{(\hat{\sigma}_{0GM}^2)_{GG}}{\hat{\sigma}_0^2} = \chi_{exp}^2 \leq \chi_{r,95\%}^2,$$

where $r$ is the redundancy of the least-square problem ($r = 70$) at the 95 per cent significance level and $(\hat{\sigma}_{0GM})_{GGS} = 2.47$ mm yr$^{-1}$. In terms of agreement between the overall solution and the azimuth constraints, the weighted RMSE of the estimated azimuth with respect to the *a priori* chosen results WRMSE $(\alpha)_{GGS} = 4.68$ (Table 3); note that WRMSE is adimensional: each residual between prior and estimated azimuth is weighted with the inverse of its variance.

(2) *15 cm yr$^{-1}$ solution (S15)*: In this case $\omega_Z$ is chosen so that the maximum velocity within the Pacific plate is 15 cm yr$^{-1}$; the



(a)



(b)
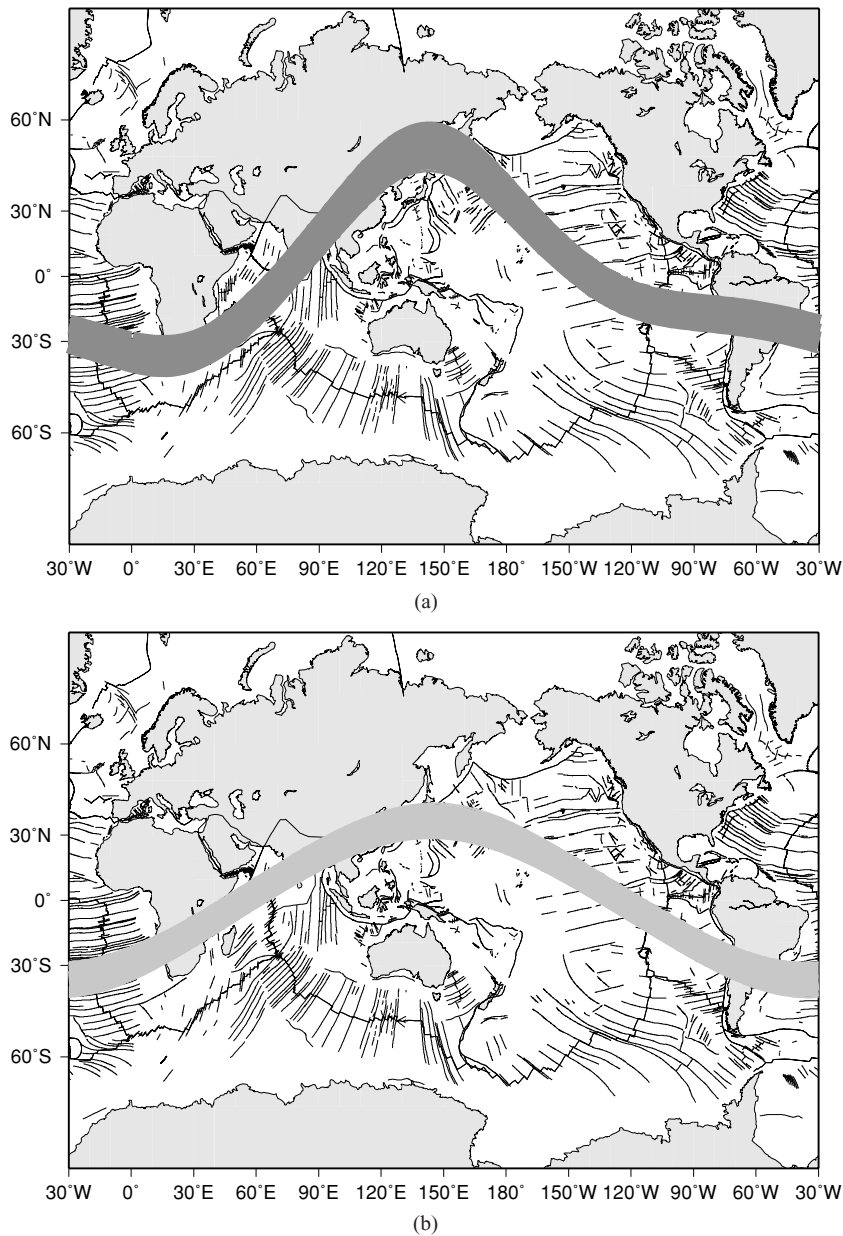
**Figure 7.** Tectonic mainstream representations (Table 5): (a) dark grey, latitude confidence interval of $\pm 7.3°$ for GGS and (b) light grey, latitude confidence interval of 6.8° obtained for S20 (PA maximum tangential velocity of 20.8 cm yr$^{-1}$ and net lithospheric rotation of 13.4 cm yr$^{-1}$ at $1\sigma$ confidence level).
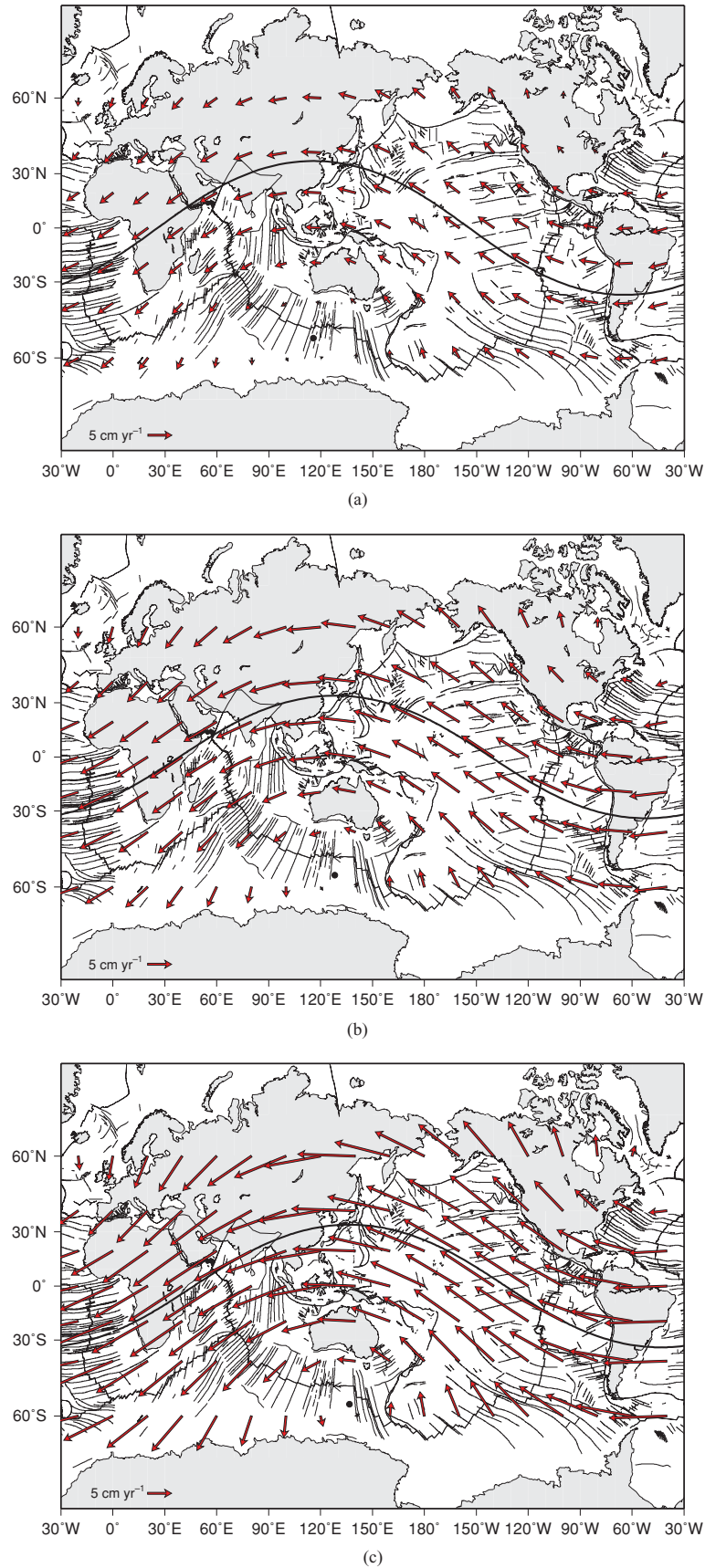
**Figure 8.** Global lithospheric net rotation, tangential velocities and equators: (a) GGS solution, maximum tangential velocity of 4.1 cm yr$^{-1}$; (b) S15, maximum tangential velocity of 8.0 cm yr$^{-1}$ and (c) S20, maximum tangential velocity of 13.4 cm yr$^{-1}$.

estimated standard deviation of unit weight of the global model $\hat{\sigma}_{0\mathrm{GM}}$ is $(\hat{\sigma}_{0\mathrm{GM}})_{15S} = 2.33$ mm yr$^{-1}$ and obviously fulfils the global test on the model too. In terms of agreement between the overall solution and the azimuth constraints, the weighted RMSE of the estimated azimuth with respect to the *a priori* chosen results WRMSE $(\alpha)_{15S} = 2.25$ (Table 3).

(3) *20 cm yr$^{-1}$ solution (S20)*: In this case $\omega_Z$ is chosen so that the maximum velocity within the Pacific plate is 20 cm yr$^{-1}$; the estimated standard deviation of unit weight of the global model $\hat{\sigma}_{0\mathrm{GM}}$ is $(\hat{\sigma}_{0\mathrm{GM}})_{20S} = 2.18$ mm yr$^{-1}$; in terms of agreement between the overall solution and the azimuth constraints, the weighted RMSE of the estimated azimuth with respect to the *a priori* chosen results WRMSE $(\alpha)_{20S} = 1.95$ (Table 3).

Comparing these solutions, some remarks may be drawn.

Even if all solutions fulfil the global test on the model, it is clearly evident that S15 and S20 exhibit a finer agreement with the geological constraints (azimuths, Eulerian equators continuity, attitude of the Pacific plate Eulerian equator). In this respect, it is also evident that S15 and S20 are quite similar, even if the Pacific plate maximum velocity difference between them (5 cm yr$^{-1}$) is about 1.5 larger than between GGS and S15 (3.8 cm yr$^{-1}$). Therefore, the agree-

ment between space geodesy solution and geological constraints seems require that Pacific plate be faster than derived in Gripp & Gordon (2002). In the same time, since solutions with faster and faster Pacific plate does not differ significantly as regards the agreement between space geodesy solution and geological constraints, it is not possible to clearly assess an upper limit for the Pacific plate velocity and for the derived plate kinematics uniquely on their basis; in fact, it is possible to retrieve other quite similar solutions with higher maximum Pacific plate velocity, but here only the S20, as hypothesized in Doglioni *et al.* (2005), and the intermediate S15 are discussed.

The main differences between GGS and S15/S20 regard the Indian and Nazca plates. In GGS at their plate boundaries significant discontinuities of the Eulerian equators are still present in latitude. In fact, if we take into account that 26° is the mean latitude discontinuity at the plate boundaries, for Nazca plate we have 25° and 41° with respect to South American and Pacific plates, respectively and for Indian plate we have 79° and 73° with respect to Eurasian and African plates respectively. Moreover, in GGS the Nazca plate moves essentially eastward, different form all other plates and the other solutions (Figs 6a, b and c). Remarkable differences are also found for the estimated net rotations, in terms of maximum

**Table 3:** Plate angular velocity components, rms and max. tangential velocities

| PLATE | | GGS $\omega$ °/Myr | rms °/Myr | V$_{tmax}$ cm/yr | rms cm/yr | S15 $\omega$ °/Myr | rms °/Myr | V$_{tmax}$ cm/yr | rms cm/yr | S20 $\omega$ °/Myr | rms °/Myr | V$_{tmax}$ cm/yr | rms cm/yr |
|---|---|---|---|---|---|---|---|---|---|---|---|---|---|
| PA | $\omega_X$ | −0.2036 | 0.0441 | | | −0.3536 | 0.0671 | | | −0.5905 | 0.1117 | | |
| | $\omega_Y$ | 0.4765 | 0.0332 | | | 0.5944 | 0.0712 | | | 0.7392 | 0.1235 | | |
| | $\omega_Z$ | −0.9066 | 0.0001 | 11.6 | 0.2 | −1.2115 | 0.0001 | 15.5 | 0.4 | −1.6153 | 0.0001 | 20.8 | 0.7 |
| NZ | $\omega_X$ | −0.1868 | 0.0372 | | | −0.3387 | 0.0635 | | | −0.5821 | 0.1107 | | |
| | $\omega_Y$ | −0.2384 | 0.0591 | | | −0.1202 | 0.0806 | | | 0.0066 | 0.1314 | | |
| | $\omega_Z$ | 0.1559 | 0.0244 | 3.8 | 0.5 | −0.1479 | 0.0231 | 4.3 | 0.7 | −0.5557 | 0.0219 | 8.9 | 0.9 |
| SA | $\omega_X$ | −0.1617 | 0.0368 | | | −0.3144 | 0.0637 | | | −0.5529 | 0.1105 | | |
| | $\omega_Y$ | 0.1010 | 0.0370 | | | 0.2176 | 0.0729 | | | 0.3618 | 0.1244 | | |
| | $\omega_Z$ | −0.3509 | 0.0203 | 4.4 | 0.3 | −0.6549 | 0.0192 | 8.4 | 0.4 | −1.0588 | 0.0180 | 13.9 | 0.7 |
| AF | $\omega_X$ | −0.0804 | 0.0282 | | | −0.2425 | 0.0623 | | | −0.4796 | 0.1100 | | |
| | $\omega_Y$ | 0.0367 | 0.0281 | | | 0.1503 | 0.0702 | | | 0.2943 | 0.1232 | | |
| | $\omega_Z$ | −0.1101 | 0.0191 | 1.6 | 0.3 | −0.4136 | 0.0183 | 5.6 | 0.5 | −0.8178 | 0.0172 | 11.0 | 0.7 |
| AR | $\omega_X$ | 0.0451 | 0.0415 | | | 0.0517 | 0.0802 | | | −0.0975 | 0.1236 | | |
| | $\omega_Y$ | 0.0425 | 0.0274 | | | 0.3119 | 0.0763 | | | 0.5407 | 0.1282 | | |
| | $\omega_Z$ | −0.0230 | 0.0291 | 0.7 | 0.4 | −0.2051 | 0.0497 | 4.2 | 0.7 | −0.5415 | 0.0540 | 8.6 | 1.0 |
| EU | $\omega_X$ | −0.1708 | 0.0358 | | | −0.3236 | 0.0632 | | | −0.5622 | 0.1104 | | |
| | $\omega_Y$ | 0.0356 | 0.0357 | | | 0.1530 | 0.0722 | | | 0.2970 | 0.1242 | | |
| | $\omega_Z$ | −0.0945 | 0.0248 | 2.2 | 0.4 | −0.3981 | 0.0234 | 6.0 | 0.5 | −0.8021 | 0.0220 | 11.4 | 0.8 |
| IN | $\omega_X$ | 0.2434 | 0.0791 | | | 0.0908 | 0.0918 | | | −0.1477 | 0.1268 | | |
| | $\omega_Y$ | 0.3011 | 0.3306 | | | 0.4180 | 0.3189 | | | 0.5623 | 0.3166 | | |
| | $\omega_Z$ | 0.0887 | 0.0884 | 4.4 | 3.5 | −0.2153 | 0.0835 | 5.3 | 2.8 | −0.6191 | 0.0783 | 9.4 | 1.7 |
| AU | $\omega_X$ | 0.3110 | 0.0477 | | | 0.1583 | 0.0699 | | | −0.0801 | 0.1138 | | |
| | $\omega_Y$ | 0.5095 | 0.0482 | | | 0.6264 | 0.0787 | | | 0.7707 | 0.1275 | | |
| | $\omega_Z$ | 0.0398 | 0.0265 | 6.7 | 0.4 | −0.2642 | 0.0250 | 7.8 | 0.8 | −0.6680 | 0.0234 | 11.4 | 1.1 |
| NA | $\omega_X$ | −0.0697 | 0.0359 | | | −0.2224 | 0.0633 | | | −0.4608 | 0.1104 | | |
| | $\omega_Y$ | 0.0124 | 0.0498 | | | 0.1293 | 0.0795 | | | 0.2736 | 0.1280 | | |
| | $\omega_Z$ | −0.3209 | 0.0403 | 3.7 | 0.5 | −0.6249 | 0.0381 | 7.5 | 0.5 | −1.0287 | 0.0358 | 12.9 | 0.7 |
| AN | $\omega_X$ | −0.0763 | 0.0140 | | | −0.0763 | 0.0132 | | | −0.0763 | 0.0124 | | |
| | $\omega_Y$ | −0.0766 | 0.0183 | | | −0.0766 | 0.0172 | | | −0.0766 | 0.0162 | | |
| | $\omega_Z$ | 0.1719 | 0.0356 | 2.3 | 0.4 | 0.1719 | 0.0336 | 2.3 | 0.4 | 0.1719 | 0.0316 | 2.3 | 0.4 |
| Net rot | $\omega_X$ | −0.0936 | 0.0330 | | | −0.2463 | 0.0619 | | | −0.4847 | 0.1097 | | |
| | $\omega_Y$ | 0.1948 | 0.0300 | | | 0.3117 | 0.0701 | | | 0.4561 | 0.1231 | | |
| | $\omega_Z$ | −0.2951 | 0.0133 | 4.1 | 0.3 | −0.5990 | 0.0127 | 8.0 | 0.4 | −1.0028 | 0.0119 | 13.4 | 0.7 |
| $\sigma_0$ | | | 2.47 | | | | 2.33 | | | | 2.18 | | |
| WRMSE | | | 4.68 | | | | 2.25 | | | | 1.95 | | |

**Table 4:** Plate rotation poles and angular velocity module.

| PLATE | GGS | | | S15 | | | S20 | | |
|---|---|---|---|---|---|---|---|---|---|
| | Lat (°) | Lon (°) | $\Omega$ °/Myr | Lat (°) | Lon (°) | $\Omega$ °/Myr | Lat (°) | Lon (°) | $\Omega$ °/Myr |
| PA | −60.2 | 113.1 | 1.0442 | −60.3 | 120.7 | 1.3950 | −59.6 | 128.6 | 1.8720 |
| NZ | 27.2 | −128.1 | 0.3406 | −22.4 | −160.5 | 0.3886 | −43.7 | 179.4 | 0.8047 |
| SA | −61.5 | 148.0 | 0.3994 | −59.7 | 145.3 | 0.7584 | −58.0 | 146.8 | 1.2481 |
| AF | −51.2 | 155.5 | 0.1412 | −55.4 | 148.2 | 0.5024 | −55.5 | 148.5 | 0.9928 |
| AR | −20.4 | 43.2 | 0.0662 | −33.0 | 80.6 | 0.3768 | −44.6 | 100.2 | 0.7714 |
| EU | −28.5 | 168.2 | 0.1985 | −48.0 | 154.7 | 0.5354 | −51.6 | 152.2 | 1.0236 |
| IN | 12.9 | 51.0 | 0.3972 | −26.7 | 77.8 | 0.4789 | −46.8 | 104.7 | 0.8493 |
| AU | 3.8 | 58.6 | 0.5982 | −22.2 | 75.8 | 0.6980 | −40.8 | 95.9 | 1.0231 |
| NA | −77.6 | 169.9 | 0.3286 | −67.6 | 149.8 | 0.6757 | −62.5 | 149.3 | 1.1600 |
| AN | 57.8 | −134.9 | 0.2031 | 57.8 | −134.9 | 0.2031 | 57.8 | −134.9 | 0.2031 |
| Net Rot | −53.8 | 115.7 | 0.3658 | −56.4 | 128.3 | 0.7188 | −56.4 | 136.7 | 1.2036 |

tangential velocities reaching 4.1 cm yr$^{-1}$ for GGS, 8.0 cm yr$^{-1}$ for S15 and 13.4 cm yr$^{-1}$ for S20 (Table 3). The net rotation poles for S15 and S20 are located quite close (approximately 450 km apart), whilst GGS net rotation pole is about 800 km from S15 pole (Table 4, Figs 8a, b and c).

In this sense, the hypothesis of the ordered lithospheric flow, according to which all plates move westward (Fig. 6 b and c), results to match better with the geological constraints, well agreeing with higher velocities and shallower asthenospheric source for the Hawaii and Society hotspot sources.

On the other hand, it is evident that at the boundaries of India and Nazca plates the continuity condition of the Eulerian equations fails, suggesting both these plates may experience significant subrotations here not considered and to reconsider the reliability of their ITRF2000 sites included into our analysis (Heflin *et al.* 2004). In this respect, two of the three considered Indian sites (BAN2 and IISC) are quite close (about 5 km apart) so that they act as a unique site; therefore, both India and Nazca plate kinematics are geodetically constrained by a minimum number of sites; moreover, doubts about ITRF2000 solution for EISL site on Nazca plate were recently proposed (Kendrick *et al.* 2003).

In order to define analytically the global lithospheric flow both according to the tectonic mainstream definition of eq. (1) (Section 4) and on the basis of the three considered solutions, the coordinates of the continuity condition points at plate boundaries were estimated as weighted mean of their values on both sides (squared areas ratio $(\frac{A_p}{A_{PA}})^2$ used as weights, Schettino (1999)) together their precisions. Then, the seven parameters (Fourier's coefficients) were preliminary least-squared estimated and tested against their precisions to assess their significance; finally, only significant parameters were estimated with their precisions, in order to define the $1\sigma$ latitude confidence interval of the tectonic mainstream for each solution (Figs 7a and b).

The mean precisions are 7.3° and 6.8° for GGS and S15/S20 respectively, corresponding to about 750–800 km of uncertainty in latitude (Table 5, bottom). Consequently, the best tectonic mainstream representation is band shaped, within this area the largest tangential motions occur (Figs 7a and b). Moreover, it is worthwhile to note that:

(i) For all the solutions $a_0$ is not significant (Table 5), so that mean latitude of the tectonic mainstream is zero.

(ii) For GGS the significant parameters are $a_1$, $b_1$, $b_2$, whilst for S15 and S20 the only significant parameters are $a_1$, $b_1$ (latitude

**Table 5.** Fourier coefficients and tectonic mainstream latitude precisions ($1\sigma$ confidence level).

| | GGS | rms | S15 | rms | S20 | rms |
|---|---|---|---|---|---|---|
| $a_0$ | 0.000 | 0.000 | 0.000 | 0.000 | 0.000 | 0.000 |
| $a_1$ | −0.606 | 0.122 | −0.508 | 0.122 | −0.506 | 0.122 |
| $b_1$ | 0.316 | 0.114 | 0.353 | 0.114 | 0.360 | 0.114 |
| $a_2$ | 0.000 | 0.000 | 0.000 | 0.000 | 0.000 | 0.000 |
| $b_2$ | −0.254 | 0.071 | 0.000 | 0.000 | 0.000 | 0.000 |
| $a_3$ | 0.000 | 0.000 | 0.000 | 0.000 | 0.000 | 0.000 |
| $b_3$ | 0.000 | 0.000 | 0.000 | 0.000 | 0.000 | 0.000 |
| | | | | | | |
| Mean precision | (°) 7.3 | rms 0.5 | (°) 6.8 | rms 0.2 | (°) 6.8 | rms 0.2 |

is simply a first-order sinusoid w.r.t. longitude) and the *tectonic mainstreams* are just equal (Table 5).

(iii) For S15 and S20 the net-rotation equators lie inside the corresponding tectonic mainstream band, defined by the $1\sigma$ latitude confidence intervals (Fig. 9).

# 7 CONCLUSIONS

The main purpose of this paper is to introduce the concept of tectonic mainstream on the basis of geological evidences and to prove its consistency by space geodesy data, in order to propose a new unified way to describe plate motions with respect to the underlying mantle. A parametric function in the form of a third-order Fourier series is hypothesized for the tectonic mainstream.

The main result of this paper is a model allowing estimation of plate kinematics on the basis of both velocities from space geodesy and geological evidences used as constraints. This model was applied by using velocities of 28 ITRF2000 sites suitably selected in stable intraplate areas leading to three possible solutions under different hypotheses about Pacific hotspot source depths, being shallower the asthenospheric source, faster the velocity of the Pacific plate. For each solution, significant parameters of the tectonic mainstream truncated Fourier series are estimated together their $1\sigma$ confidence interval.

All three reconstructions are confirming (i) the tectonic mainstream and (ii) the net rotation of the lithosphere. In the GGS case, the westward drift is only an average rotation, that is, some plates
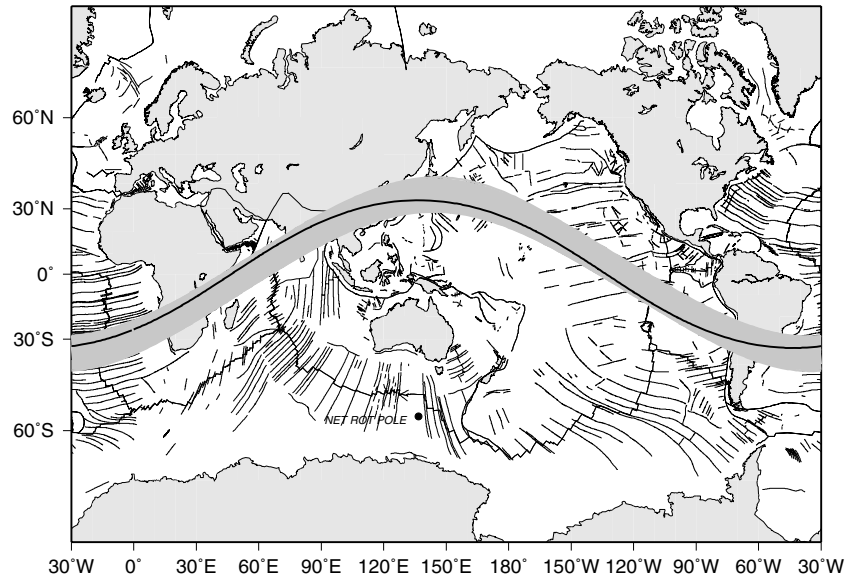
**Figure 9.** The net rotation equator lies within the tectonic mainstream latitude band, example relative to S20 solution.

(Nazca, Cocos, Juan de Fuca) still move eastward relative to the mantle. Assuming faster Pacific motions as the asthenospheric source of the hotspots would allow, the net rotation increases to a complete polarization in the remaining 2 solutions (S15 and S20), which match remarkably better with the geological constraints (Table 3). Moreover, for S15 and S20 the analytical expressions of the *tectonic mainstreams* are remarkably simpler than hypothesized, just reducing to a first-order sinusoid in longitude, quite close to the corresponding net-rotation equators.

The shear wave splitting technique (e.g. Savage 1999) is an independent tool for detecting the seismic anisotropy in the asthenosphere, that is considered the preferential orientation of olivine crystals in a sheared flowing mantle (Silver & Holt 2002). The direction of the anisotropy of between lithosphere and underlying mantle (e.g. Fischer *et al.* 1998; Montagner 2002) aligns quite consistently with the absolute plate motions reconstructions, apart along subduction zones or other mantle anomalies.

Nevertheless, since solutions with faster and faster Pacific plate does not differ significantly as regards the agreement between space geodesy solution and geological constraints, it is not possible to assess an upper limit for the Pacific plate velocity and for the derived plates kinematic on their basis, and additional hypotheses should be introduced.

In this respect, even if the occurrence of a westerly polarized lithosphere motion cannot be considered at present a controversial phenomenon (Ricard *et al.* 1991; Gripp & Gordon 2002, and reference therein, this paper), we feel that its origin is not yet completely clear, because it may be due to different combined effects hard to separate. As previously noted, a mean lithospheric rotation rather than a global phenomenon has been so far preferred (e.g. Ricard *et al.* 1991) because it preserves the angular momentum of the Earth without rapidly decelerating its rotation speed. However, it has recently been shown (Scoppola *et al.* 2006) that a global lithospheric rotation is physically feasible, although at variable velocities among the different plates. According to this recent model (Scoppola *et al.* 2006), plate tectonics would occur with the combination of a rotating planet under tidal torque, efficient internal convection, and lateral viscosity variations at the lithosphere-mantle interface where are supposed to

occur thin hydrate layers with very low viscosity. The viscosity of the upper asthenosphere is still unknown, but the effective viscosity should be about 1000 times lower when measured for a horizontal shear with respect to vertical loading as simulated in classical post-glacial rebound studies (e.g. Scoppola *et al.* 2006). Moreover, new petrological and geophysical evidences are emerging of a very low viscosity between 100–150 km at the lithosphere base, in the low velocity zone (LVZ) representing the upper asthenosphere (e.g. Panza 1980; Hirth & Kohlstedt 1996; Holtzman *et al.* 2003; Rychert *et al.* 2005; Thybo 2006). This layer is usually neglected and considered as a whole with the underlying higher viscosity lower asthenosphere. Although we do not want to force the reader to accept the faster kinematic models (S15 and S20), which may be refined in further investigations, we underline that a global net rotation is more coherent with the geological and geophysical asymmetries which support more a complete rotation of the lithosphere rather than only a mean rotation.

About the tidal role, a evidence is that the latitude range of the estimated tectonic *mainstream* is about the same of the Moon maximum declination range ($\pm 28°$) during the nutation period ($\approx 18.6$ yr). Further indications come from the fact that the induced geopotential variations and the solid Earth tide modeling (McCarthy & Petit 2004) generate maximum amplitudes of the Earth bulges ($\approx 30$ cm) propagating progressively within the same latitude range (Biagi *et al.* 2005). In particular, the track of the semi-diurnal bulge crest is about directed from E to W, as small circles moving from latitudes $28°$ to $18°$, when the Moon moves from maximum to minimum declinations (the same happens at negative latitudes for the opposite bulge), thus suggesting a role of rotational and tidal drag effects (Bostrom 1971)

For the next future, two different problems have to be faced such as:

(i)    The discussion about the relationships between the plate motions model and future realization of TRF.

(ii)    The investigation about the physical phenomena, possibly astronomical, triggering the form of plates stream and, therefore, of the tectonic mainstream.

Moreover, possible model enhancement (with particular concern to the lithospheric net rotation estimate) considering different source depths (thus different velocities for fixed surface tracks) for additional reliable hotspots have to be exploited.

## ACKNOWLEDGMENTS

## REFERENCES

Altamimi, Z., Sillard, P. & Boucher, C., 2002. ITRF2000: A new release of the International Terrestrial Reference Frame for earth science applications *J. geophys. Res.,* **107**(B10), 2214, doi:10.1029/2001JB000561.

Altamimi, Z., Sillard, P. & Boucher, C., 2003. The impact of no-net-rotation condition on ITRF2000, *Geophys. Res. Lett.,* **30**(2), 1064, doi:10.1029/2002GL016279.

Anderson, D.L., 2000, Thermal state of the upper mantle; no role for mantle plumes, *Geophys. Res. Lett.,* Vol. 27, 22, 3623–3626.

Anderson, D.L., 2005. Scoring hotspots; the plume & plate paradigms: in *Plates, Plumes and Paradigms*, pp. 31–54, eds Foulger, G.R., Natland, J.H., Presnall, D.C. & Anderson, D.L., GSA Sp. Paper 388.

Argus, D.F. & Gordon, R.G., 1991. No-net-rotation model of current plate velocities incorporating plate motion model NUVEL-1, *Geophys. Res. Lett.,* **18**, 2038–2042.

Barzaghi, R., Borghi, A., Crespi, M., Pietrantonio, G. & Riguzzi F., 2004. GPS permanent network solution: the impact of temporal correlations, *Proceedings of the V Hotine-Marussi Symposium on Mathematical Geodesy*, Vol. 127, pp. 179–183, ed. Sansò, F., Springer-Verlag, Berlin, Heidelberg, New York.

Biagi, L., Pietrantonio, G. & Riguzzi, F., 2005. Tidal and polar modeling effect on regional GPS networks, poster presented at EGU 2005 General Assembly, Vienna.

Bonatti, E., 1990. Not so hot 'hot spots' in the oceanic mantle, *Science,* **250**, 107–111.

Bostrom, R.C., 1971. Westward displacement of the lithosphere, *Nature,* **234**, 356–538.

Courtillot, V., Davaille, A., Besse, J. & Stock J., 2003. Three distinct types of hotspot in the Earth's mantle, *Earth planet. Sci. Lett.,* **205**, 295–308.

Cuffaro, M., Caputo, M. & Doglioni, C., 2004. On the sub-rotation of a plate, *J. Virtual Explor.,* **14**(2), 1–15, Electronic Edition.

Davies, G.F., 1988. Ocean bathymetry and mantle convection: 1. large-scale flow and hotspots, *J. geophys. Res.,* **93**, 10 467–10 480.

DeMets, C., Gordon, R.G., Argus, F. & Stein, S., 1990. Current plate motions, *Geophys. J. Int.,* **101**, 425–478.

DeMets, C., Gordon, R.G., Argus, F. & Stein, S., 1994. Effect of recent revisions to the geomagnetic reversal time scale on estimates of current plate motions, *Geophys. Res. Lett.,* **21**, 2121–2194.

Dermanis, A., 2001. Global Reference Frames: Connecting Observation to Theory and Geodesy to Geophysics, IAG Scientific Assembly.

Dermanis, A., 2002. The rank deficiency in estimation theory and the definition of reference frames, *Proceedings of V Hotine-Marussi Symposium on Mathematical Geodesy,* Vol. 127, pp. 145–156, ed. Sanso', F., IAG Symposia, Springer-Verlag, Berlin, Heidelberg, New York.

Doglioni, C., 1990. The global tectonic pattern, *J. Geodyn.,* **12**, 21–38.

Doglioni, C., 1993. Geological evidence for a global tectonic polarity, *J. geol. Soc. Lond.,* **150**, 991–1002.

Doglioni, C., Harabaglia, P., Merlini, S., Mongelli, F., Peccerillo, A. & Piromallo, C., 1999. Orogens and slabs vs their direction of subduction, *Earth Sci. Rev.,* **45**, 167–208.

Doglioni, C., Carminati, E. & Bonatti, E., 2003. Rift asymmetry and continental uplift, *Tectonics,* **22**(3), 1024, doi:10.1029/2002TC001459.

Doglioni, C., Green, D. & Mongelli, F., 2005. On the shallow origin of hotspots and the westward drift of the lithosphere, in *Plates, Plumes and Paradigms*, pp. 735–749, eds Foulger, G.R., Natland, J.H., Presnall, D.C. & Anderson, D.L., GSA Sp. Paper 388.

Drewes, H. & Meisel, B., 2003. An Actual Plate Motion and Deformation Model as a Kinematic Terrestrial Reference System, Geotechnologien Science Report No. 3, 40–43, Potsdam.

Fischer, K.M., Fouch, M.J., Wiens, D.A. & Boettcher, M.S., 1998. Anisotropy and Flow in Pacific Subduction Zone Back-arcs, *Pure appl. geophys.,* **151**, 463–475.

Forsyth, D. & Uyeda, S., 1975. On the relative importance of driving forces of plate motion, *Geophys. J. R. astr. Soc.,* **43**, 163–200.

Foulger, G.R., Natland, J.H., Presnall, D.C. & Anderson, D.L., 2005. *Plates, Plumes and Paradigms*, GSA Sp. Paper 388, 1–861.

Gordon, R.G., 1995. Present plate motion and plate boundaries, *Glob. Earth Phys., AGU Ref. Shelf,* **1**, 66–87.

Gripp, A.E. & Gordon, R.G., 2002. Young tracks of hotspots and current plate velocities, *Geophys. J. Int.,* **150**, 321–361.

Heflin, M. *et al.*, 2004. http://sideshow.jpl.nasa.gov/mbh/series.html.

Hirth, G. & Kohlstedt, D.L., 1996. Water in the oceanic upper mantle: implications for rheology, melt extraction and the evolution of the lithosphere, *Earth planet. Sci. Lett.,* **144**, 93–108.

Holtzman, B.K., Groebner, N.J., Zimmerman, M.E., Ginsberg, S.B. & Kohlstedt, D.L., 2003. Stress-driven melt segregation in partially molten rocks, *G3,* **4**, 8607, doi:10.1029/2001GC000258.

Kendrick, E., Bevis, M., Smalley, Jr. R., Brooks, B., Barriga Vargas, R., Laur*i*a, E. & Souto Fortes, L.P., 2003. The Nazca–South America Euler vector and its rate of change, *J. South Amer. Earth Sci.,* **16**, 125–131.

Knopoff, L. & Leeds, A., 1972. Lithospheric Momenta and the Deceleration of the Earth, *Nature,* **237**(2), 93–95.

Le Pichon, X., 1968. Sea-floor spreading and continental drift, *J. geophys. Res.,* **73**(12), 3661–3697.

McCarthy, D.D. & Petit, G., 2004. IERS Conventions (2003), IERS Technical Note No. 32, Verlag des Bundesamts für Kartographie uns Geodäsie, Frankfurt am Main.

Montagner, J.-P., 2002. Upper mantle low anisotropy channels below the Pacific Plate, *Earth planet. Sci. Lett.,* **202**, 263–274.

Morgan, W.J., 1971. Convection plumes in the lower mantle, *Nature,* **230**, 42–43.

Natland, J.H. & Winterer, E.L., 2005. Fissure control on volcanic action in the Pacific, in *Plates, Plumes and Paradigms*, eds Foulger, G.R., Natland, J.H., Presnall, D.C. & Anderson, D.L., GSA Sp. Paper 388,

Norton, I.O., 1995. Plate motions in the North Pacific; the 43 Ma non event, *Tectonics,* **14**, 1080–1094.

O'Connell, R., Gable, C.G. & Hager, B., 1991. Toroidal-poloidal partitioning of lithospheric plate motions, in *Glacial Isostasy, Sea-Level and Mantle Rheology*, Vol. 334, pp. 535–551, eds Sabadini, R., Boschi, E., Kluwer Academic Publisher, Dordrecht, The Netherlands.

Panza, G., 1980. Evolution of the Earth's lithosphere, in *Mechanisms of Continental Drift and Plate Tectonics*, pp. 75–87, eds Davies, P.A. & Runcorn, S.K., Academic Press.

Ranalli, G., 2000. Westward drift of the lithosphere: not a result of rotational drag, *Geophys. J. Int.,* **141**, 535–537.

Ricard, Y., Doglioni, C. & Sabadini, R., 1991. Differential rotation between lithosphere and mantle: a consequence of lateral viscosity variations, *J. geophys. Res.,* **96**, 8407–8415.

Ritsema, J. & Allen, R.M., 2003. The elusive mantle plume, *Earth planet. Sci. Lett.,* **207**, 1–12.

Rychert, C.A., Fischer, C.M. & Rondenay, S., 2005. A sharp lithosphere–asthenosphere boundary imaged beneath eastern North America, *Nature,* **436**, 542–545.

Savage, M.K., 1999. Seismic anisotropy and mantle deformation: What have we learned from shear wave splitting?, *Rev. Geophys.,* **37**(1), 65–106.

Schettino, A., 1999. Computational methods for calculating geometric parameters of tectonic plates, *Comput. Geosci.,* **25**, 897–907.

Scoppola, B., Boccaletti, D., Bevis, M., Carminati, E. & Doglioni, C., 2006, The westward drift of the lithosphere: a rotational drag?, *Bull. Geol. Soc. Am.,* **118,** 1/2, 199–209, doi:10.1029/2004TC001634.

Searle, R.C., 1986. GLORIA investigations of oceanic fracture zones: comparative study of the trasform fault zone, *J. geol. Soc., Lond.,* **143,** 743–756.

Silver, P.G. & Holt, W.E., 2002. The mantle flow field beneath western North America, *Science,* **295,** 1054–1057.

Smith, A.D., 1993. The continental mantle as a source for hotspot volcanism, *TerraNova,* **5,** 452–460.

Smith, A.D. & Lewis, C., 1999. The planet beyond the plume hypothesis, *Earth Sci. Rev.,* **48,** 135–182.

Stein, S., 1993. Space geodesy and plate motions, *Amer. Geophys. Union, Geodyn. Series,* **23,** 5–20.

Thybo, H., 2006. The heterogeneous upper mantle low velocity zone, *Tectonophysics,* **416,** 53–79.

Von Kármán, T. & Biot, M.A., Metodi matematici nell'ingegneria, Einaudi edition, 1951, in Italian.

Wessel, P. & Smith, W.H.F., 1995. *The Generic Mapping Tools (GMT) version 3.0*, Technical Reference & Cookbook, SOEST/NOAA.